INTERNATIONAL JOURNAL OF AUTOMOTIVE AND MECHANICAL ENGINEERING
ISSN: 2229-8649 e-ISSN: 2180-1606
VOL. 20, ISSUE 3, 2023, 10659 – 10670
DOI: https://doi.org/10.15282/ijame.20.3.2023.09.0823

RESEARCH ARTICLE

Comparison Analysis Between PI and Adaptive Controllers for DC-DC Converter of Hybrid Energy Storage Systems in Electric Vehicles

M. Islam[1], M. Abdullah[1,*], A.F.A. Ghaffar[1] and S. Ahmad[1,2]

[1]Department of Mechanical and Aerospace Engineering, International Islamic University Malaysia, 53100, Kuala Lumpur, Malaysia
[2]College of Engineering and Technology, University of Doha for Science and Technology, Doha, Qatar

ABSTRACT - A power converter is one of the important components in a hybrid electric vehicle (HEV), where it has a strong nonlinear dynamic due to the variation of load demand from different driving modes, namely acceleration, braking and cruising. To adapt with the nonlinearities, this work proposes the use of direct model reference adaptive control (DMRAC) to regulate its operation in tracking the load and current demand of the HEV. To validate the response, the control performance is benchmarked with the commonly used traditional PI controller. The system model includes a battery with a supercapacitor, and its controller was constructed using the MATLAB Simulink platform. Simulation results show that DMRAC provides better performance as compared to the PI controller in two cases, which are tracking the current and load demands according to the root mean square error (RMSE) analysis. Nevertheless, in the presence of disturbance, it is noted that DMRAC is only effective in tracking the current demand while requiring some time to adapt and surpass the PI controller in tracking the load demand. Based on these findings, it can be justified that the DMRAC has the potential to become a good alternative approach to control the HEV power converters, specifically in the presence of disturbance.

ARTICLE HISTORY

Received	:	05th May 2023
Revised	:	17th Aug 2023
Accepted	:	28th Aug 2023
Published	:	09th Oct 2023

KEYWORDS
Adaptive control;
DC-DC converter;
PI controller;
Electric vehicle;
Supercapacitor

1.0 NOMENCLATURE

$\hat{k}_r$	estimation of k_r	k_x	adjustable gain for states
$\hat{k}_x$	estimation of k_x	γ_r	adaptation gain rate for reference inputs
$\dot{k}_r / dk_r$	derivative of k_r	γ_x	adaptation gain rate for states
$\dot{k}_x / dk_x$	derivative of k_x	I_{Batt}	battery current
K_I	integral gain.	I_{SC}	SC current
K_P	proportional gain	C	Controller
X_a	actual states	C_o	DC bus capacitor
X_d	desired states	R_o	DC resistor
X_m	states of reference model	e	error between two states
X_s	states of plant	r	reference input.
$\dot{e}$	error dynamics	u	control input
k_r	adjustable gain for reference input	I_0	DC bus current

2.0 INTRODUCTION

Nowadays, a high dependency on fossil fuels has triggered several negative impacts on the environment, such as exposure to CO_X, SO_X, and NO_X gases, which can worsen the current greenhouse effect [1]. As the price of fuel is increasing [2], the demand for alternative energy, such as electricity, has become more favourable especially if it is generated from renewable energy. Hence, there are many policies and legislations that have been set up to focus on the awareness of Electric Vehicle (EV) [3]. As compared to the traditional internal combustion engine, it is well known that EVs can provide better carbon emissions, fuel efficiency, and electro-mechanical systems [4-6].

The EV powertrain consists of multiple crucial parts, including energy storage systems (ESSs), powertrain controllers, electric motors, transmission, and power converters [7]. In general, EVs can be classified based on their ESS architectures [8], and for hybrid electric vehicles (HEV), there are two ESSs that are frequently used namely primary ESSs and secondary ESSs. The primary ESS provide the necessary power to satisfy the load demand, while secondary ESSs acts as support if the load demand exceeds the capability of the primary ESS. For instance, in the work of Lundin [9], the flywheel is used as a secondary ESSs due to its high discharge rate to improve the overall energy density of the battery. Similarly, Ostadi and Kazerani use a supercapacitor (SC) as the secondary ESS to boost the overall specific power to prolong the battery life [10].

*CORRESPONDING AUTHOR | M. Abdullah| ✉ mohd_abdl@iium.edu.my

The lithium-ion battery is considered a suitable energy storage system for EV, which has great demand due to its high energy efficiency, high specific power and long life cycle [11]. In general, the energy density, power density, and nominal voltage of lithium-ion battery range are 100-270 Wh/kg, 250-680 W/kg and 3.2-3.7 V respectively [12]. As there is no straightforward rule, each manufacturer can design the battery capacity for its EV. For example, the Tesla Model X-100 can travel 371 miles with 100 kWh battery capacity, whereas the Smart Fortwo has a battery of 17.6 kWh capacity to run 65 miles only [13]. Besides, in general, the range of energy density, pulse load, charge/discharge time and nominal voltage of commercial SC span from 1-5 Wh/kg, 1-100 A, 1-10 seconds and 2.3-3 V, respectively [11, 14]. AFS Trinity Power Corporation has commercially introduced a prototype of a hybrid electric vehicle that combines both battery and supercapacitor to meet the power demand of the vehicle [15]. Nevertheless, this newly adapted concept is not widely available in the market, even though researchers find it to be significantly promising.

In an HEV, a regular switching between the two ESSs is continuously required due to the drive cycle, and therefore, to cope with that, a power converter is needed to convert different types of supply current, such as AC to DC and DC to DC, as well as stepping the voltage or current up and down. Since DC-DC converters primarily deal with regulating the voltage or current, batteries are frequently charged or discharged using these converters due to their effectiveness [16], compactness, and cost-effectiveness [17]. Three different topologies are commonly discussed for DC-DC converters: buck, boost, and buck-boost converters. To adhere to the design specifications, a feedback control is commonly used to ensure that the pulse width modulation (PWM) input signals are properly supplied and distributed to satisfy the voltage or current demand.

In general, there are different types of control algorithms that can be used for this system [18]. The most common one is from the family of proportional-integral-derivative (PID) control due to their ease of design, affordable cost, and straightforward implementation [16]. Nevertheless, these controllers have a well-known drawback in terms of robustness, especially for a wide range of operating points and highly nonlinear dynamic since their gains are often tuned based on fixed global operational points [18-20]. Consequently, the system's performance may become worse, especially in the presence of uncertainties or load disturbances [21]. This issue has triggered the use of nonlinear controllers for power converter operation.

As for the nonlinear controller, Sliding Mode Control (SMC) is quite popular among power converter applications. Its prime advantages are simplified algorithmic formulation [18], the ability to handle discontinuous signals [22] and model uncertainty [23]. However, as reported in the literature, SMC often suffers from chattering issues that can be detrimental to a system [24, 25]. Besides, its irregular switching frequency can also lead to a potential electromagnetic interference [16, 26]. In some cases, SMC occasionally produces an inaccurate steady-state response due to its inability to follow the output voltage [27].

The feedback linearization method is one of the proposed solutions that can overcome SMC's chattering problem and steady-state error [28]. It exhibits its efficiency in terms of dynamic performance by offering robustness against varying load fluctuations [29]. Although the feedback linearization updates its linear model frequently for adaptation, the nonlinear features are usually ignored when constructing the model [30]. Another improvement method for SMC is by integrating it with the backstepping control approach, which is very effective in avoiding the chattering problem [31]. Nevertheless, it is reported that a user must adhere to a strictly followed systematic framework and is required to use system parameters precisely to prevent system uncertainty, which is practically not feasible in many applications [18].

To fill in the research gap, this work proposes the use of Direct Model Reference Adaptive Control (DMRAC) as an alternative algorithm to support the power demand of a DC-DC Converter by extending the work of [28]. The controller is implemented in a hybrid ESS that consists of a battery and supercapacitor for a specific HEV. The primary contribution of this work is the novel use of the DMRAC in a DC-DC converter to track the power consumption of a HEV, which has not yet been investigated in the literature. The second contribution will be on the formal comparison and analysis of the proposed controller with the traditional PI in tracking two parameters, which are the demanded power and current in the presence of system disturbances. This paper is organized such that Section 1 introduces the literature review and the objective of the work. Section 2 describes the circuit topologies that are used to construct the state-space equation. Section 3 presents the DMRAC control framework. Section 4 discusses the simulation results, and Section 5 concludes the work.

3.0 HYBRID ESS MODEL

In this work, the HESS model is constructed based on the combination of supercapacitor (SC) and battery pack, where each energy source is regulated by the respective bidirectional DC-DC converters (BDC). As the primary focus of this work is on the distribution of power according to load demand using two different control algorithms, the 3-phase motor and power inverter (also known as DC-AC Converter) have not been considered, though. Figure 1 shows all the general components of the HEV powertrain system. The buck-boost converter is used to extract and supply the power to the SC, while the boost converter is only used to extract the power from the battery pack. Figure 2 shows the schematic circuit of the boost converter, which includes an inductor, L_1, with two insulated gate bipolar transistors (IGBT) D_1 and D_2. Additionally, Figure 2(b) demonstrates the circuit diagram of a buck-boost converter, consisting of an inductor, L_2, with two IGBTs as D_3 and D_4 that deal with SC power demand. To run the 3-phase BLDC electric motor, a continuous voltage of 48 V is required, and thus, these DC-DC converters are connected in parallel to a voltage source, DC Bus [32].

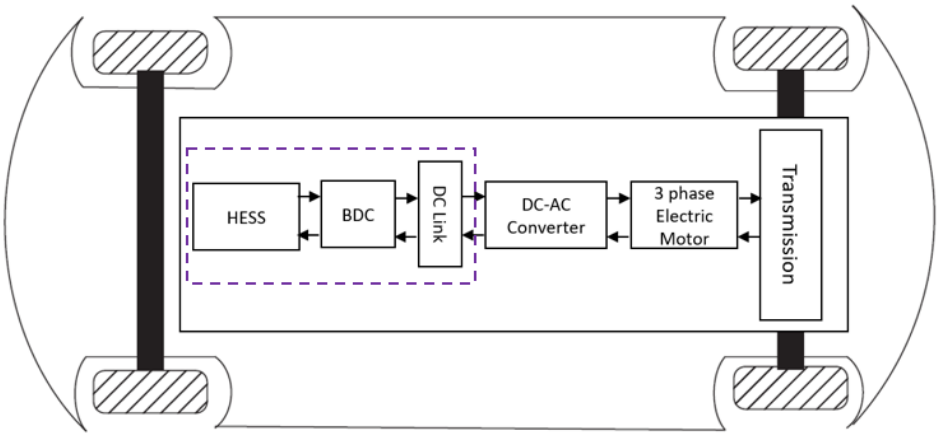

Figure 1. Block diagram of an HEV powertrain

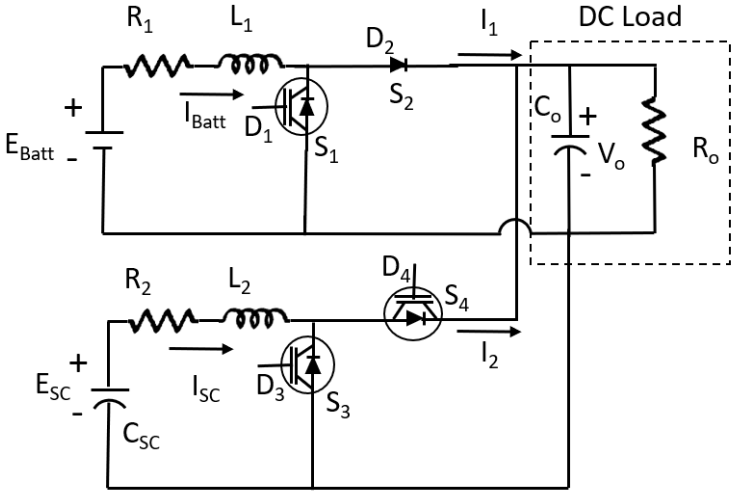

Figure 2. Circuit model of the Buck-Boost Converter with a battery and boost converter with the SC

Figure 2 contributes to developing a mathematical model of the complete circuit as [33]:

$$\dot{I}_{Batt} = -\frac{R_1}{L_1} I_{Batt} + \frac{E_{Batt}}{L_1} - \frac{V_o}{L_1}(1 - D_1) \tag{1}$$

$$\dot{I}_{SC} = -\frac{R_2}{L_2} I_{SC} + \frac{E_{SC}}{L_2} - \frac{V_o}{L_2} D \tag{2}$$

$$\dot{V}_o = \frac{I_{Batt}}{C_o}(1 - D_1) + \frac{I_o}{C_o} - \frac{I_{SC}}{C_o} D \tag{3}$$

$$I_o = I_1 + I_2 \tag{4}$$

Here, $D = (1 - D_3) \cdot T + D_4 \cdot (1 - T)$ where T is 0 for the buck mode and 1 for the boost mode of the buck-boost converter. Noted that when the vehicle runs traction mode, both the converters extract power from battery pack and SC where D_1, D_3 and D_4 are active. On the other hand, in braking mode, only D_1 is active, whereas D_3 and D_4 are inactive. In Eq. (1) to (4), D_1, D_2, D_3 and D_4 are the duty ratios in the respective IGBTs. Table 1 shows different driving modes of the vehicle along with the IGBTs status.

Table 1. Driving modes and IGBTS status

Mode	Active	Inactive
Acceleration or Traction	D_1, D_3 and D_4	–
Brake	D_1	D_3 and D_4

In this work, the MATLAB/Simulink Supercapacitor model example [34] is used as a plant with minor modifications, specifically in the Power Management System (PMS), which is explained in the next subsection to meet the motor voltage requirement. Table 2 lists the power converter parameters as well as the properties of the HESS for the simulation work that represents the similar properties of other works [35].

Table 2. HESS component properties and power converters' parameters [34]

Components and their properties	Values
Battery Pack	
Rated capacity	6.6 Ah
Cell nominal voltage	3.3 V
No. of cell in series	8
No. of cell in parallel	1
Response time	30s
Initial SOC	100%
Supercapacitors	
Rated voltage	16 V
Initial voltage	16 V
Capacitance	500 F
No. of parallel capacitors	1
No. of series capacitors	6
Equivalent DC series resistance	2.1 mΩ
DC Bus	
DC bus voltage	48 V
DC load capacitor	0.11 F
DC load resistance	25 Ω
Boost and buck-boost converter	
Switching frequency	40×10^{3} Hz
Inductance	1×10^{-3} H

4.0 POWER MANAGEMENT SYSTEM

A power management system (PMS) is needed to distribute the necessary amount of power to the motor from the HESS. In addition, it is also used to improve battery safety, energy consumption, efficiency, and system dynamics [32]. There are various types of strategies that can be used for the PMS, such as rule-based strategy [32], filtration-based strategy [36], "all or nothing" control strategy [37], fuzzy logic strategy [38] and model predictive strategy [39]. For the simplicity of simulation and better adaptability according to a drive cycle, the rule-based approach is adopted in this work, as shown in Figure 3. This technique enables the battery pack to supply power if the load demand from the motor, P_d, exceeds zero. In the meantime, the SC remains constant until P_d meets the P_{min} cut-off that is considered as 1.5 kW since the total system is considered to be run for 600 s only, which will make the battery and SC depleted. In addition, the power fluctuation is prominently visible at around 1.5 kW for this drive cycle. Note that the cut-off power is changeable according to system run time, power storage or the rate of power discharge. In the meantime, once P_d surpasses the P_{min} limit, the SC supplies the remaining demand of the power as $(P_d - P_{min})$. To guarantee effective power conversion, the state of charge (SOC) of the SC is closely monitored during this period. As a result, the SC voltage managed to remain between $0.5V_{SC_{max}}$ and $V_{SC_{max}}$. In this case, the operational condition for the battery pack has been considered between 20% and 90% of the SOC.

5.0 CONTROL STRATEGIES

This section discusses the design of PI and DMRAC controllers. This chapter describes the control strategies in two subsections: Adaptive control algorithm and PI control algorithm.

5.1 Adaptive Control Algorithm

One of the advantages of DMRAC is that no internal model is needed to represent a plant rather than the measured states are used to compute the control input. Since this work is an extension of [28], the detailed algorithm's development of DMRAC can be found in the paper. Therefore, only a brief overview is provided in this work. Figure 4 shows the overall control structure for DMRAC, which consists of four major components, namely the reference model, plant, controller, and adjustment mechanism. The main goal of this controller is to force the plant to behave similarly to the reference model output by imposing an adaptive mechanism via the gain selection.

The first step is to set up a reference model to produce the desired performance of the HESS. In this study, the reference model is designed so that it can generate an output signal with 0.03 s rise time, 0.06 s settling time and 0% of overshoot.

These parameters can be represented in a transfer function form and then be converted into state space form using the *tf2ss* function in MATLAB. Thus, the reference model parameters can be represented as:

$$A_m = \begin{bmatrix} -200 & -9000 \\ 1 & 0 \end{bmatrix}, B_m = \begin{bmatrix} 1 \\ 0 \end{bmatrix}, C_m = [0 \quad 9000] \tag{5}$$

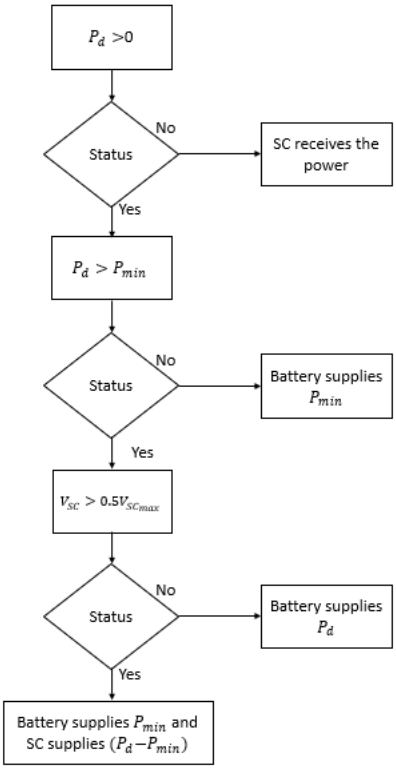

Figure 3. Rule Based PMS

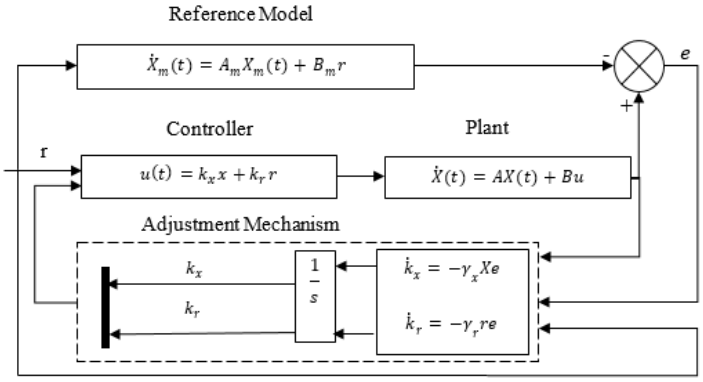

Figure 4. DMRAC workflow

The parameter in Eq. (1) can then be formulated in a state format as:

$$\dot{X}_m(t) = A_m X_m(t) + B_m r \tag{6}$$

where, A_m and B_m must be positive and greater than zero, and the input is fed from a reference signal r. At the same time, the control law also receives the reference input and tuned input from the adjustment mechanism to generate input for the plant so that it can provide similar behavior as the reference model. Hence, the control law is designed by considering the input as:

$$u(t) = k_x X_s + k_r r \tag{7}$$

where, X_s is the system states, k_x and k_r are defined as the gains for states and reference inputs, respectively, where they need to be tuned to obtain a satisfactory performance.

The control objective is to ensure that $X(t)$ will converge to $X_m(t)$ to obtain the desired performance. Nevertheless, the fact that A and B are regarded as unknown parameters, the following formula is used to compute the error between the reference model and the plant:

$$e(t) = X_s - X_m \tag{8}$$

The X_s can be expanded by substituting the input u in Eq. (7) to the general form of $AX_s + Bu$. Utilizing the time derivative of Eq. (8) with the substitution of Eq. (7), the rearranged version of the error rate can then be integrated to handle error dynamics as follows:

$$\dot{e}(t) = (A + Bk_x)X_s - A_mX_m + Bk_r r - B_m r \tag{9}$$

In the meantime, to minimize the error dynamics, A_m and B_m should be defined as:

$$A + Bk_x = A_m \tag{10}$$

$$Bk_r = B_m \tag{11}$$

Subsequently, a new control law based on estimation can be defined as Eq. (12) since the parameters of the converter are considered unknown:

$$u = \hat{k}_x(t)X_s + \hat{k}_r(t)r \tag{12}$$

where $\hat{k}_x(t)$ is the estimation of k_x and $\hat{k}_r(t)$ is the estimated by k_r. Hence:

$$A_m - B\hat{k}_x(t) = A \tag{13}$$

$$B\hat{k}_r(t) = B_m \tag{14}$$

The substitution of A in Eq. (13) and B_m in Eq. (11) to Eq. (9) can lead to a new closed-loop error dynamic as:

$$\dot{e}(t) = A_m e - B(\tilde{k}_x - \tilde{k}_r) \tag{15}$$

Here, $(\hat{k}_x - k_x)$ and $(\hat{k}_r - k_r)$ has been replaced by $\tilde{k}_x$ and $\tilde{k}_r$ respectively.

To estimate these values, the adjustment mechanism will minimize the error between output from the plant and the reference model. Since ensuring system stability is one of the crucial parts of designing this controller, a Lyapunov function has been considered as shown in Eq. (16).

$$V(e, \tilde{k}_x, \tilde{k}_r) = \frac{1}{2\gamma}e^2 + \frac{1}{2\gamma}\tilde{k}_x{}^2 + \frac{1}{2\gamma}\tilde{k}_r{}^2 \tag{16}$$

$$\dot{V} = \frac{1}{\gamma}\left(A_m e^2 - B\tilde{k}_x Xe - B\tilde{k}_r re - \tilde{k}_x\dot{\tilde{k}}_x - \tilde{k}_r\dot{\tilde{k}}_r\right) \tag{17}$$

In both Eq. (18) and (19), adaptation gain rates, γ_r and γ_x are considered since they can converge the error [35]. Importantly, to ensure system stability, $\dot{V}$ must be negative semi-definite and hence, both $\dot{\hat{k}}_r$ and $\dot{\hat{k}}_x$ should be defined as:

$$\dot{\hat{k}}_r = -\gamma_r Bre \tag{18}$$

$$\dot{\hat{k}}_x = -\gamma_x BXe \tag{19}$$

As a result, Eq. (17) can be represented as:

$$\dot{V} = A_m e^2 \tag{20}$$

Since A_m is considered as negative, $\dot{V}$ is preferably considered as negative semi-definite. As a result, the system can be defined as stable. Thus, the error dynamics as described in Eq. (15) is modified when Eq. (18) and Eq. (19) go through the integration process and hence, $\dot{\hat{k}}_r$ and $\dot{\hat{k}}_x$ are updated accordingly, as well as the control input.

5.2 PI Control Algorithm

The PI control approach is commonly used with DC-DC converter because of its simplicity in design and ability to ensure promising performance. Since the methodology of the PI controller is already well known, only the final form is presented. The PI controller, *C* can be defined as follows:

$$C = K_P + \frac{K_I}{s} \tag{21}$$

$$u_C(t) = \left(K_P + \frac{K_I}{s}\right)e \tag{22}$$

where, $e(t) = X_d - X_a$

5.3 DMRAC Tuning and Analysis

Typically, controller performance is determined by the gains; consequently, selecting an appropriate gain is a vital step for controllers. To choose the appropriate gains for PI and DMRAC, a variety of approaches can be considered. The trial-and-error approach has been taken into consideration in this work for both PI and DMRAC control algorithms. The aim is to select the gains that give less spike and fluctuation. For DMRAC, the values both for γ_x and γ_r must be positive according to the control design method and, therefore, γ_x and γ_r ranges are [0, 10] and [0, 1] respectively. Noted that the value of γ_r should be changed in a slower rate in order to allow the controller to adapt slowly and accurately.

Figure 5 demonstrates that both the rate of change of gain dk_x and dk_r in DMRAC are significantly influenced by the values of adaptation gain γ_x and γ_r. In this case, γ_r was varied between 0.5, 0.05, 0.005, and 0.0005. It is noticed that dk_x changes more smoothly when γ_r is 0.0005, as shown in Figure 5(d). Noted that when γ_r was 0.005, higher spikes in changing dk_x are prominently visible if Figure 5(c), whereas the spikes of comparatively lower magnitude are found in Figure 5(d) when γ_r was 0.0005. Also, it is observed that higher values of γ_x lead to higher fluctuations in Figure 6. The abrupt peaks of dk_x are prominently visible due to the larger values of γ_x that allows space for further analysis, as referred to Figure 6(a). Figure 6(b) shows the rate of changes of dk_r due to the variations of γ_x. In this instance, the rate of change of dk_r increases as the value of γ_x increases, and it rises higher in every 10s. Hence, considering the system stability, for the smoothest rate of change of dk_r, the value for γ_x has been chosen as 1 where γ_r = 0.0005.

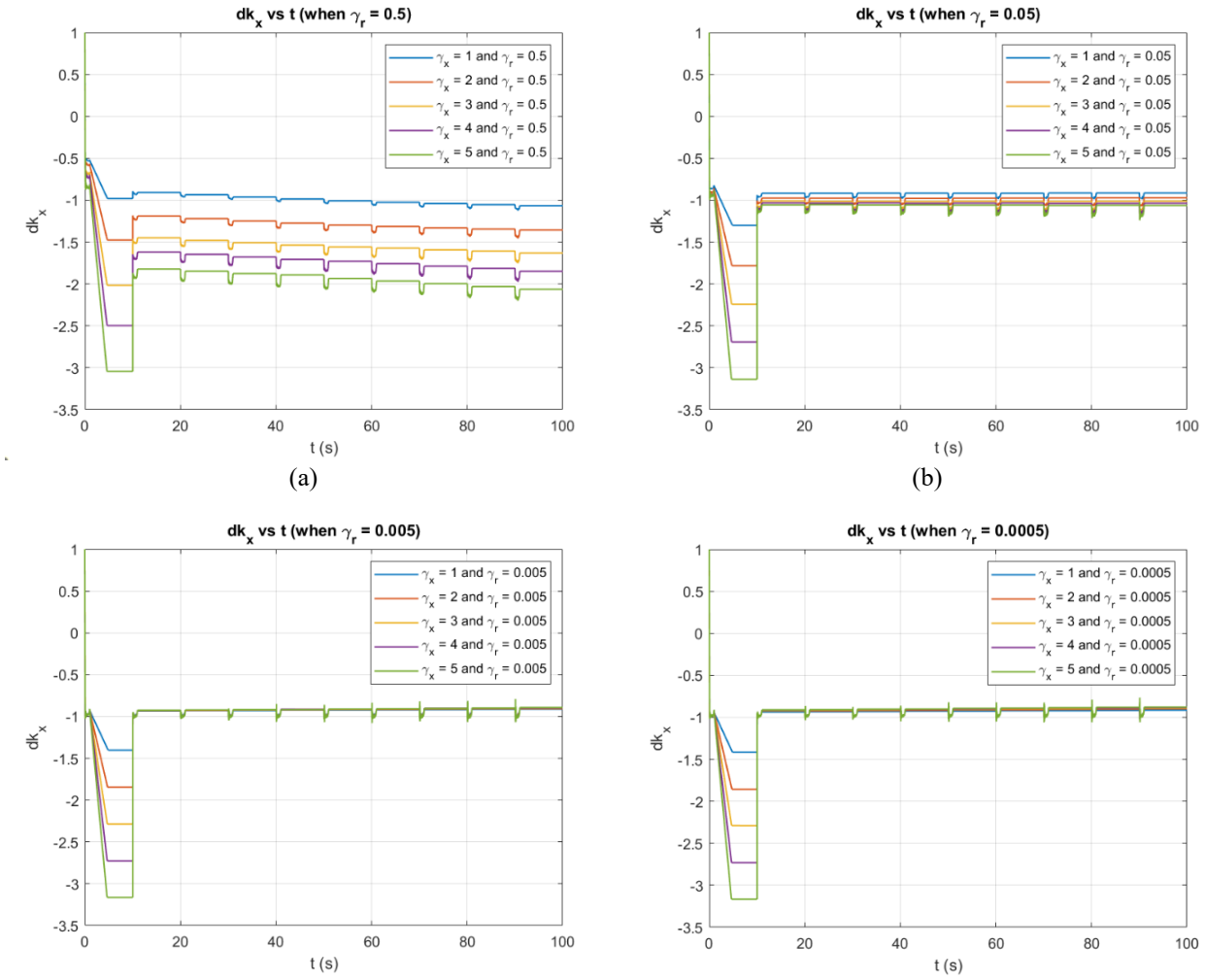

Figure 5. Impact of $\boldsymbol{\gamma_r}$ on $\boldsymbol{dk_x}$ when it is (a) 0.5, (b) 0.05, (c) 0.005 and (d) 0.0005

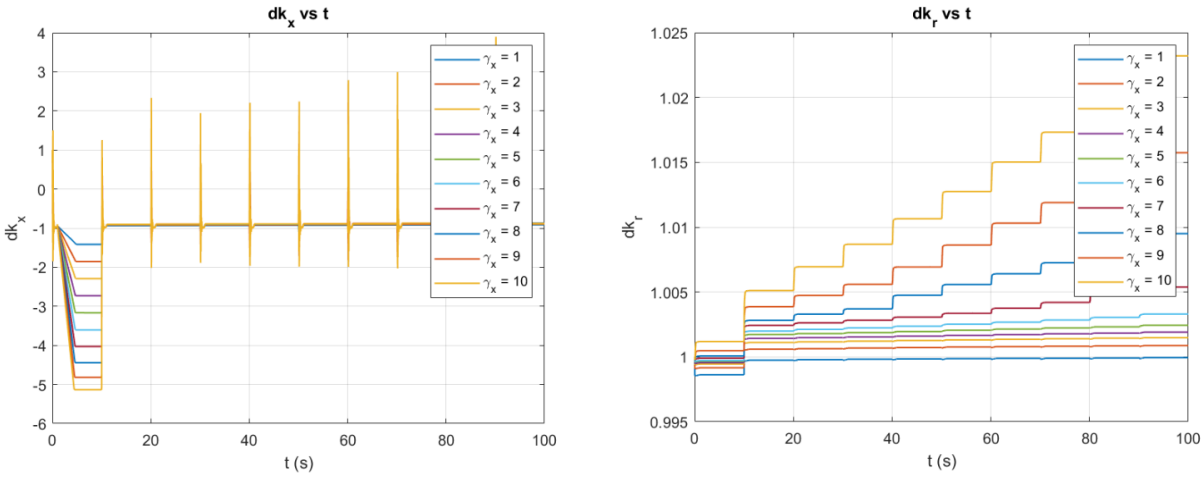

(a) (b)

Figure 6. Impact of $\boldsymbol{\gamma_x}$ on the rate of changes of (a) $\boldsymbol{dk_x}$ and (b) $\boldsymbol{dk_r}$

5.4 PI Gains Tuning

In order to tune the gain of PI, a similar trial-and-error method has been adopted due to its simplicity. In this trial-and-error method, both K_I and K_p gain of PI controller has been considered between 0 and 100 based on extreme system response. However, the demonstration of the gain analysis has been avoided in this work since the minute changes of PI gains have a significant impact on the current system performance and at the same time, the analysis is not the contribution to this work. Table 3 highlights the final gains of PI and adjustable gains of DMRAC considered in this study.

Table 3: Gains of PI and DMRAC control algorithm

PI	DMRAC
K_P= 1.5	γ_r = 0.0005
K_I = 1	γ_x = 1

6.0 RESULTS AND DISCUSSION

This section compares the performance of two control approaches, PI and DMRAC, based on several factors as defined by the performance index. Two different cases have been considered, which are current tracking for SC and power demand tracking, that is explained later in this section.

As mentioned previously, the battery supports 1.5 kW or below; the rest of the power is extracted from the SC as long as SC is able to supply the rest of the demand. Here, the PI controller has been considered to deal with the current, $I_{Batt,}$ since the battery's power output is presumed to remain constant around 1.5 kW. On the other side, SC must sustain the rest of the power, as described previously. It regulates its current, I_{SC}, to track the remaining power. Since I_{SC} varies often, both DMRAC and PI controllers have been examined for monitoring it. Two simulation instances are therefore taken into consideration to examine the controllers' current tracking performance: (a) in the absence of disturbance and (b) in the presence of disturbance.

Since supplying sufficient power is important for the motor to run smoothly, power demand tracking should necessarily be considered to analyze the controllers' performance. Figure 7 shows the system's block diagrams to illustrate the operational flow between the converters and controllers, where I_{Batt} and I_{SC} have been tracked. Thus, the output current is denoted by I_{SC}, the disturbance is denoted by d, and u represents the control input. To investigate the tracking performance of the controllers, random disturbance has been considered in the system for every 10 s period, and hence, I_{SC} supply from SC that is influenced by disturbance has been tracked as illustrated in Figure 7(b), since I_{SC} fluctuates continuously while the rate of changes of I_{Batt} is not as high as I_{SC}.

Figure 8 shows the status of the current, voltage and SOC of battery pack and SC during the transient period when no disturbance affects the system. Here, their statuses have been prioritized because they are three key components of a PMS. Figure 9 demonstrates the I_{SC} tracking and $(P_d - P_{min})$ demand tracking of both the controllers. When power demand reaches its peak of 2.5 kW, as illustrated in Figure 9(b), the required I_{SC} increases, as shown in Figure 9(a). Since the voltage drops and the supercapacitor keeps up with $(P_d - P_{min})$ demand, the I_{SC} demand rises as the voltage drops, as shown in Figure 8(b). In this instance, disturbances to the system have not been considered; hence both DMRAC and PI are able to ensure smooth tracking.

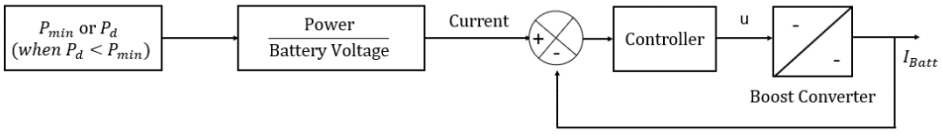

(a)

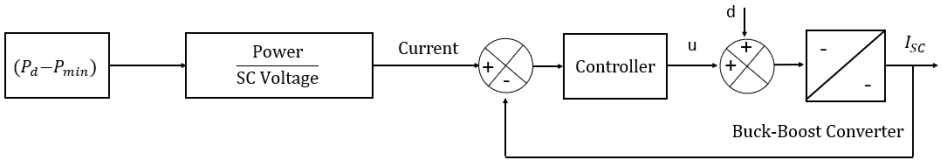

(b)

Figure 7. Workflow of a controller with a DC-DC converter when (a) I_{Batt} and (b) I_{SC} are supplied from battery pack and SC, respectively

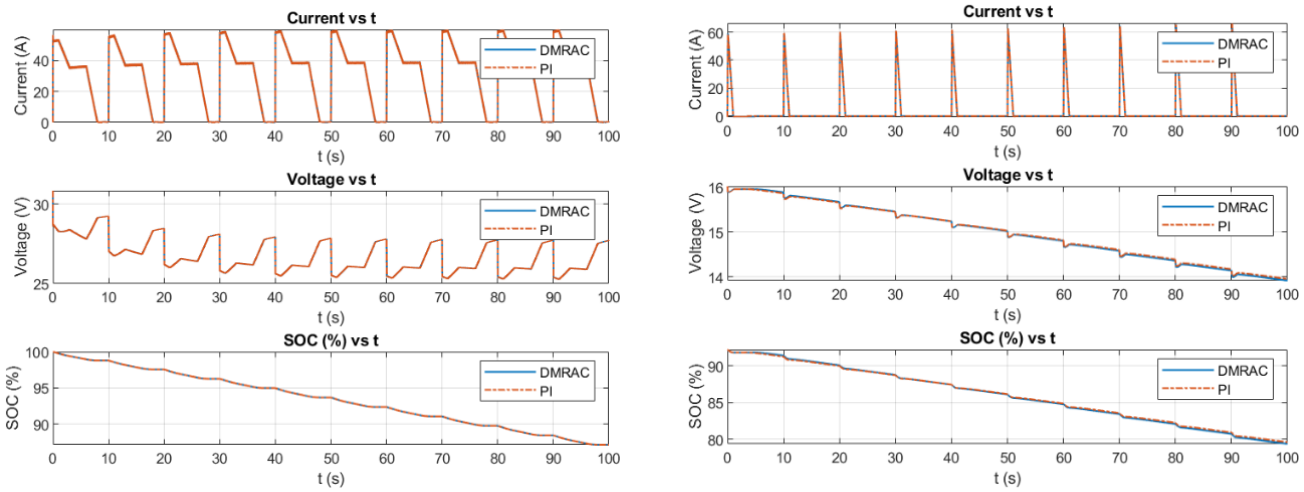

(a) (b)

Figure 8. Status of current, voltage and SOC in the (a) battery pack and (b) SC in the absence of disturbance to the system

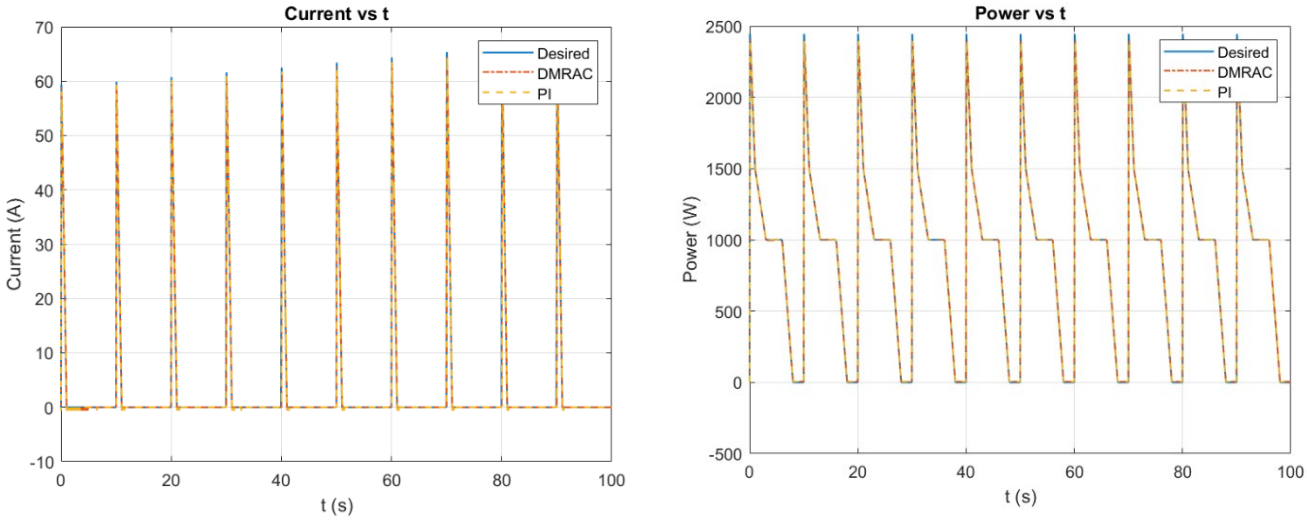

(a) (b)

Figure 9. Controllers' performance in tracking (a) I_{SC} and (b) $(\boldsymbol{P_d - P_{min}})$ in the absence of disturbance in the system

Figure 10 also depicts the current and load demands with time; however, in this case, disturbance in the system has been taken into account. So, it is found that both DMRAC and PI perform deteriorate as compared to when there is no disturbance. For a better understanding of the controllers' performance, Figure 11 demonstrates I_{SC} tracking for a limited transient response between 150s and 151s as a zoomed-in version of Figure 10(a). It is important to note that the simulation confirms that DMRAC performs gradually better over time, as predicted by the algorithm's theory. It is also noted,

nevertheless, that when the system is affected by the disturbance, DMRAC does not outperform the PI controller in terms of power tracking. In this study, DMRAC is implemented for I_{SC} tracking and therefore, it is unable to adjust itself according to the considered to handle to track power demand directly. It is outside the capability of this controller to track power in accordance with a given reference.

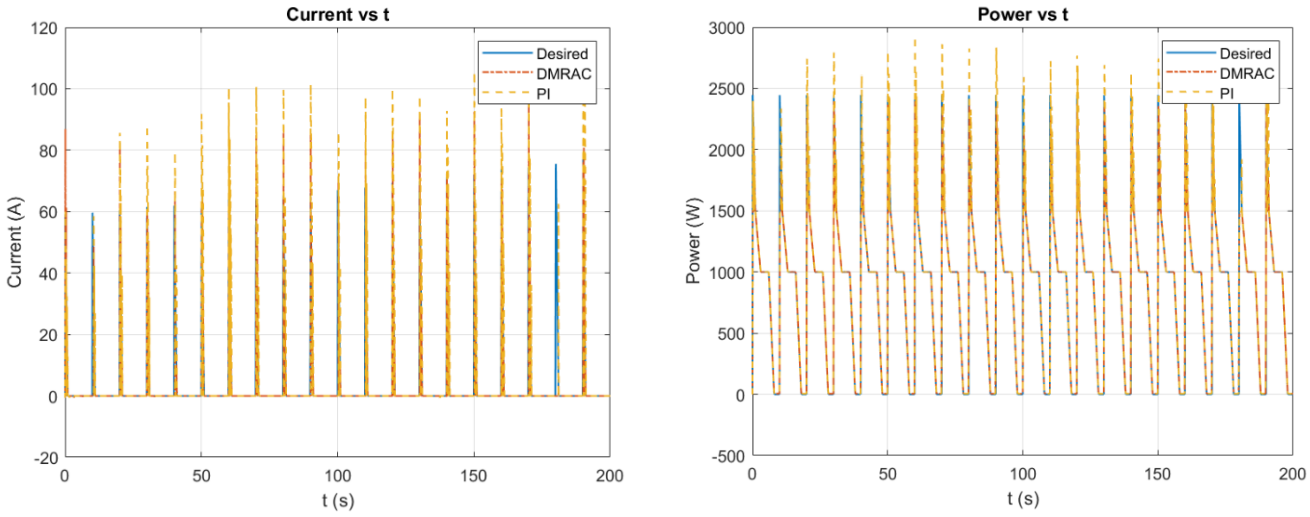

(a) (b)

Figure 10. Controllers' performance in tracking (a) I_{SC} and (b) $(\boldsymbol{P_d - P_{min}})$ in the presence of disturbance in the system

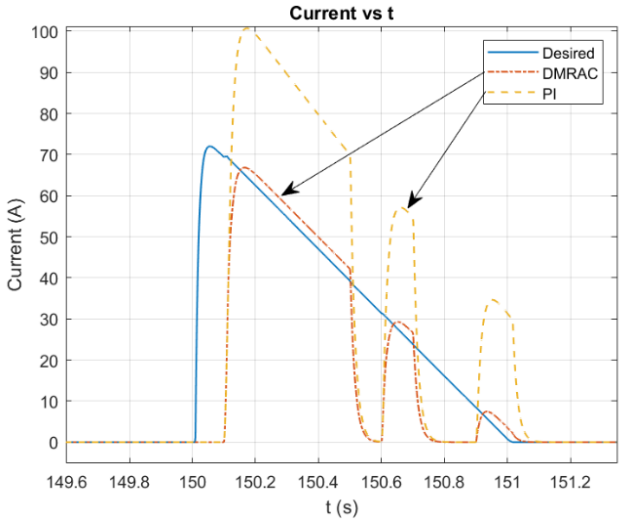

Figure 11. I_{SC} tracking between 150 s and 151 s

Since Figure 9 and Figure 10 are unable to exhibit the controllers' tracking errors explicitly, root mean square (RMS) error has been taken into consideration in order to understand the controllers' performances, as shown in Table 4. When there is no disturbance, DMRAC outperforms the PI controller, where DMRAC is 11% and 13% more accurate in current tracking and power tracking, respectively. DMRAC further demonstrates its superior performance than PI controller when it is the case of current tracking in the presence of disturbance and shows a 14% more accurate result. However, due to the previously mentioned limitation of DMRAC as not directly dealing with power tracking, PI performs better in the scenario of power tracking when there is system disturbance, with an RMSE of 1.64%.

Table 4. RMS error along with DMRAC and PI control approaches

Cases	RMS error	
	PI (%)	DMRAC (%)
In absence of disturbance		
Power tracking	0.17	0.04
Current tracking	0.45	0.40
In presence of disturbance		
Power tracking	1.64	2.77
Current tracking	31.69	27.32

Table 5 demonstrates the characteristics of system responses such as peak time, rising time, settling time and overshoot when the controllers are adopted. While analyzing the performance of the two control approaches, it is found that the discrepancies are not particularly notable. As the DMRAC requires some time to learn and performs better, system response characteristics may not be appropriate to support their efficacy.

Table 5. Characteristics of system response in the presence of DMRAC and PI control algorithm

Properties	Controllers	
	PI	DMRAC
Peak time (s)	0.99	0.99
Rise time (s)	0.06	0.067
Settling time (s)	0.12	0.13
Overshoot (%)	0	0

By definition, the DMRAC approach is appropriate for a system that is affected by the disturbance. This work has considered the effects of an uncertain disturbance that has an impact on system performance. Figure 10 demonstrates that in the presence of a disturbance, the transient duration is longer than in the absence of a disturbance, where the DMRAC algorithm gradually improves over time. DMRAC struggles to demonstrate its effectiveness initially, but as time passes, its performance improves, as it is demonstrated in Figure 11. As a result, Figure 10 has been highlighted prominently in Table 4 to emphasize its characteristic of improving performance with respect to time. The PI controller, in contrast, is a linear controller that relies on fixed gains and cannot adapt over time. Even while it provides satisfactory performance, it fails to outperform the DMRAC approach in both instances, even though it demonstrates the potentiality as a viable controller.

Conversely, the DMRAC approach is more difficult to develop than the PI control approach because the DMRAC algorithm requires an additional reference model at first. Another difficulty is making sure the system has Lyapunov stability. As the control does not change, the system stability checking has been neglected in this study. On the other hand, a PI controller's implementation with a system and selection of an appropriate gain is comparatively simpler than the DMRAC method. However, DMRAC has the advantage of adjusting to a changing environment when dealing with uncertainty, which proves its efficacy as a promising controller for this application.

7.0 CONCLUSIONS

This work offered a formal comparison between PI and DMRAC control algorithms for HESS power distribution in EV. Essentially, a PMS is considered to ensure power supply from two different power sources so that it can consistently meet the load requirement. The DMRAC algorithm has thus been introduced to make sure the load demand throughout power distribution at different conditions. The findings demonstrate that DMRAC provides accurate, current tracking both in the absence and presence of disturbance. The DMRAC algorithm outperforms the PI controller in terms of performance indexes. Hence, even if the system is disturbed externally by any means, the DMRAC algorithm can be a suitable control method for current tracking in a buck-boost converter of a hybrid ESS in an EV. Using the buck-boost converter of a HESS-powered EV in the power distribution, this work fills a gap in the literature where the DMRAC algorithm has not previously been taken into consideration. In the future, this work can be validated using a Hardware-In-Loop (HIL) system, which will be able to determine its viability on a real-time EV.

8.0 ACKNOWLEDGEMENT

This work is funded by the Ministry of Higher Education Malaysia through the Fundamental Research Grant Scheme (FRGS/1/2019/TK07/UIAM/03/1).

9.0 REFERENCES

[1] S. Paraschiv and L. S. Paraschiv, "Trends of carbon dioxide (CO2) emissions from fossil fuels combustion (coal, gas and oil) in the EU member states from 1960 to 2018," *Energy Reports,* vol. 6, pp. 237-242, 2020.

[2] B. H. Kreps, "The rising costs of fossil-fuel extraction: an energy crisis that will not go away," *American Journal of Economics and Sociology,* vol. 79, no. 3, pp. 695-717, 2020.

[3] J. Y. Yong, V. K. Ramachandaramurthy, K. M. Tan, and N. Mithulananthan, "A review on the state-of-the-art technologies of electric vehicle, its impacts and prospects," *Renewable and sustainable energy reviews,* vol. 49, pp. 365-385, 2015.

[4] R. Ghorbani, E. Bibeau, and S. Filizadeh, "On conversion of hybrid electric vehicles to plug-in," *IEEE Transactions on Vehicular Technology,* vol. 4, no. 59, pp. 2016-2020, 2010.

[5] A. Emadi, Y. J. Lee, and K. Rajashekara, "Power electronics and motor drives in electric, hybrid electric, and plug-in hybrid electric vehicles," *IEEE Transactions on Industrial Electronics,* vol. 55, no. 6, pp. 2237-2245, 2008.

[6] Z. Amjadi and S. S. Williamson, "Power-electronics-based solutions for plug-in hybrid electric vehicle energy storage and management systems," *IEEE Transactions on Industrial Electronics,* vol. 57, no. 2, pp. 608-616, 2009.

[7] K. Ç. Bayindir, M. A. Gözüküçük, and A. Teke, "A comprehensive overview of hybrid electric vehicle: Powertrain configurations, powertrain control techniques and electronic control units," *Energy Conversion and Management,* vol. 52, no. 2, pp. 1305-1313, 2011.

[8] A. Ghosh, "Possibilities and challenges for the inclusion of the electric vehicle (EV) to reduce the carbon footprint in the transport sector: A review," *Energies,* vol. 13, no. 10, p. 2602, 2020.
[9] J. Lundin, "Flywheel in an all-electric propulsion system," Ph.D Thesis, Uppsala Universitet, Sweeden, 2011.
[10] A. Ostadi and M. Kazerani, "A comparative analysis of optimal sizing of battery-only, ultracapacitor-only, and battery–ultracapacitor hybrid energy storage systems for a city bus," *IEEE Transactions on Vehicular Technology,* vol. 64, no. 10, pp. 4449-4460, 2014.
[11] F. Ju, Q. Zhang, W. Deng, and J. Li, "Review of structures and control of battery-supercapacitor hybrid energy storage system for electric vehicles," *Advances in Battery Manufacturing, Service, and Management Systems,* pp. 303-318, 2016.
[12] K. Liu, K. Li, Q. Peng, and C. Zhang, "A brief review on key technologies in the battery management system of electric vehicles," *Frontiers of Mechanical Engineering,* vol. 14, pp. 47-64, 2019.
[13] M. K. Hasan, M. Mahmud, A. A. Habib, S. Motakabber, and S. Islam, "Review of electric vehicle energy storage and management system: Standards, issues, and challenges," *Journal of Energy Storage,* vol. 41, p. 102940, 2021.
[14] M. Horn, J. MacLeod, M. Liu, J. Webb, and N. Motta, "Supercapacitors: A new source of power for electric cars?" *Economic Analysis and Policy,* vol. 61, pp. 93-103, 2019.
[15] F. Naseri, S. Karimi, E. Farjah, and E. Schaltz, "Supercapacitor management system: A comprehensive review of modeling, estimation, balancing, and protection techniques," *Renewable and Sustainable Energy Reviews,* vol. 155, p. 111913, 2022.
[16] R.-J. Wai and L.-C. Shih, "Design of voltage tracking control for DC–DC boost converter via total sliding-mode technique," *IEEE Transactions on Industrial Electronics,* vol. 58, no. 6, pp. 2502-2511, 2010.
[17] İ. Yazici and E. K. Yaylaci, "Fast and robust voltage control of DC–DC boost converter by using fast terminal sliding mode controller," *IET Power Electronics,* vol. 9, no. 1, pp. 120-125, 2016.
[18] T. K. Nizami and C. Mahanta, "An intelligent adaptive control of DC–DC buck converters," *Journal of the Franklin Institute,* vol. 353, no. 12, pp. 2588-2613, 2016.
[19] E. Sahin, M. S. Ayas, and I. H. Altas, "A PSO optimized fractional-order PID controller for a PV system with DC-DC boost converter," In 2014 16th International Power Electronics and Motion Control Conference and Exposition, 2014, pp. 477-481.
[20] M. F. Adnan, M. A. M. Oninda, M. M. Nishat, and N. Islam, "Design and simulation of a DC-DC boost converter with PID controller for enhanced performance," *International Journal of Engineering Research & Technology (IJERT),* vol. 6, no. 09, pp. 27-32, 2017.
[21] L. Po, L. Ruiyu, S. Tianying, Z. Jingrui, and F. Zheng, "Composite adaptive model predictive control for DC–DC boost converters," *IET Power Electronics,* vol. 11, no. 10, pp. 1706-1717, 2018.
[22] B. M. David and K. Sreeja, "A Review of sliding mode control of DC-DC converters," *International Research Journal of Engineering and Technology,* vol. 2, no. 4, pp. 1382-1386, 2015.
[23] V. Utkin, "Sliding mode control of DC/DC converters," *Journal of the Franklin Institute,* vol. 350, no. 8, pp. 2146-2165, 2013.
[24] Y. Massaoudi, D. Elleuch, J. P. Gaubert, D. Mehdi, and T. Damak, "A new backstepping sliding mode controller applied to a dc-dc boost converter," *International Journal of Power Electronics and Drive Systems,* vol. 7, no. 3, p. 759, 2016.
[25] N. Benbaha, F. Zidani, M.-S. Nait-Said, S. E. Zouzou, S. Boukebbous, and H. Ammar, "DSPACE validation of improved backstepping optimal energy control for photovoltaic systems," In 2018 6th International Renewable and Sustainable Energy Conference (IRSEC), 2018, pp. 1-6.
[26] S. Saadatmand, P. Shamsi, and M. Ferdowsi, "The heuristic dynamic programming approach in boost converters," In 2020 IEEE Texas Power and Energy Conference (TPEC), 2020, pp. 1-6.
[27] N. Abjadi, A. Goudarzian, G. R. Arab Markadeh, and Z. Valipour, "Reduced-order backstepping controller for POESLL DC–DC converter based on pulse width modulation," *Iranian Journal of Science and Technology, Transactions of Electrical Engineering,* vol. 43, pp. 219-228, 2019.
[28] M. Islam, A. F. Abdul Ghaffar, E. Sulaeman, M. M. Ahsan, A. Z. Kouzani, and M. P. Mahmud, "Performance analysis of PI and DMRAC algorithm in buck–boost converter for voltage tracking in electric vehicle using simulation," *Electronics,* vol. 10, no. 20, p. 2516, 2021.
[29] J. Liu, W. Ming, and F. Gao, "A new control strategy for improving performance of boost DC/DC converter based on input-output feedback linearization," In 2010 8th World Congress on Intelligent Control and Automation, 2010, pp. 2439-2444.
[30] L.-K. Yi, J. Zhao, and D. Ma, "Adaptive backstepping sliding mode nonlinear control for buck DC/DC switched power converter," In 2007 IEEE International Conference on Control and Automation, 2007, pp. 1198-1201.
[31] S. K. Ghosh, T. K. Roy, M. A. H. Pramanik, and M. A. Mahmud, "Design of nonlinear backstepping double-integral sliding mode controllers to stabilize the DC-bus voltage for DC–DC converters feeding CPLs," *Energies,* vol. 14, no. 20, p. 6753, 2021.
[32] Z. Song, J. Hou, H. Hofmann, J. Li, and M. Ouyang, "Sliding-mode and Lyapunov function-based control for battery/supercapacitor hybrid energy storage system used in electric vehicles," *Energy,* vol. 122, pp. 601-612, 2017.
[33] B. Fatah, M. Chokri, Y. Hamed, H. Naceur, and H. Hassan, "Hybrid modelling of energy management system in electric traction," In International Conference on Control, Engineering & Information Technology, 2012, vol. 1, pp. 192-197.
[34] P. C. Blaud and L.-A. Dessaint. "Supercapacitor Model." MathWorks [Online]. Available: https://au.mathworks.com/help/sps/ug-/supercapacitor-model.html [Accessed July 7, 2023].
[35] A. Ranjan and S. B. Bodkhe, "Modified energy management strategy for HESS in electric vehicle," In 2021 9th IEEE International Conference on Power Systems (ICPS), 2021, pp. 1-6.
[36] M. Hadartz and M. Julander, *Battery-supercapacitor energy storage*. Chalmers University of Technology Gothenburg, Sweden, 2008.
[37] A.-L. Allegre, A. Bouscayrol, and R. Trigui, "Influence of control strategies on battery/supercapacitor hybrid energy storage systems for traction applications," In 2009 IEEE Vehicle Power and Propulsion Conference, 2009, pp. 213-220.
[38] Z. Song, H. Hofmann, J. Li, J. Hou, X. Han, and M. Ouyang, "Energy management strategies comparison for electric vehicles with hybrid energy storage system," *Applied Energy,* vol. 134, pp. 321-331, 2014.
[39] M. Hannan, F. Azidin, and A. Mohamed, "Multi-sources model and control algorithm of an energy management system for light electric vehicles," *Energy Conversion and Management,* vol. 62, pp. 123-130, 2012.